Few-Body Systems 16, 101–125 (1994)

Few-Body Systems

Photon Scattering on Quasi-Free Neutrons in the Reaction $\gamma d \to \gamma' np$ and Neutron Polarizabilities

M. I. Levchuk[1], A. I. L'vov[2], and V. A. Petrun'kin[2]

[1] B. I. Stepanov Institute of Physics, Belorussian Academy of Sciences, F. Scarina Prospect 70, 220602 Minsk, Belarus

[2] P. N. Lebedev Physical Institute, Russian Academy of Sciences, Leninsky Prospect 53, Moscow 117924, Russia

Abstract. The possibility to obtain information on γn scattering at intermediate energies from the reaction $\gamma d \to \gamma' np$ is analyzed. To this aim, the differential cross section $d^3\sigma/d\Omega_{\gamma'}\, d\Omega_n\, dE_n$ and the scattering asymmetry with linearly polarized photons are calculated at photon energies 100 to 400 MeV in the diagrammatic approach. The pole diagrams of the impulse approximation are evaluated with realistic γn and γp scattering amplitudes. One-loop diagrams with np rescattering in the final state and with meson-exchange and isobar currents are taken into account as well. The main contribution to the differential cross section $d^3\sigma/d\Omega_{\gamma'}\, d\Omega_n\, dE_n$ in the kinematics of quasi-free γn scattering arises from the neutron pole diagram. The correction due to other diagrams is typically -30% to -10% and decreases with increasing photon energy and momentum transfer. The sensitivity of the cross sections to the magnitude of the neutron electric polarizability and to the sign of the $\pi^0 \to 2\gamma$ decay constant is demonstrated.

1 Introduction

Up to recent years, the elastic photon scattering by neutrons (hereafter simply "γn scattering") at low and intermediate energies has never been studied experimentally. Both the lack of dense neutron targets and the absence of advanced theoretical analyses of photon scattering by neutrons bound in nuclei prevented to do this. The very first (though indirect) data on γn scattering have been obtained by the Göttingen-Mainz group [1]. They measured the differential cross section of the reaction

$$\gamma + d \to \gamma' + n + p \tag{1}$$

in the neutron quasi-free peak region smeared over the energy interval of $E_\gamma \sim 80$–130 MeV and found the following value for the neutron electric polarizability,

$$\alpha_n = 10.7^{+3.3}_{-10.7}, \tag{2}$$

in the units of 10^{-4} fm^3 used for the polarizabilities throughout the paper. The uncertainties in (2) were smaller than those in results obtained in earlier investigations of neutron scattering by nuclei [2–6]. The possibility to determine the polar-

izability α_n from the data on inelastic photon-deuteron scattering (1) has been pointed out in the work [7], in which the differential cross section $d^3\sigma/d\Omega_{\gamma'}\, d\Omega_n\, dE_n$ of the reaction (1) has been calculated in the distorted-wave impulse approximation within the diagrammatic approach [8, 9]; it has been shown to be sensitive to the hadron structure parameters involved through the subprocess of γn scattering, in particular to the neutron polarizability α_n and the relative sign of πNN and $\pi^0\gamma\gamma$ coupling constants.

Generally, one can expect a close similarity between mechanisms of γn scattering and those of the much better studied γp scattering, especially near the nucleon resonances. However, there are some important differences that deserve a special experimental investigation. For example, due to the absence of the Thomson term in the low-energy γn scattering amplitude, the corresponding differential cross section is very sensitive to the contribution of t-channel π^0-exchange at energies below the pion photoproduction threshold. If the π^0-decay constant $F_{\pi^0\gamma\gamma}$ has a standard sign, which is opposite to the sign of the πNN coupling constant, $g_{\pi NN}$, the contribution of the π^0-exchange increases the differential cross section of backward γn scattering by $\sim +100\%$ at the photon energy of about 100 MeV, whereas it provides the change of only $\sim -10\%$ in the case of γp scattering [10]. Hence, data on γn scattering enable one to determine the relative sign of $F_{\pi^0\gamma\gamma}$ and $g_{\pi NN}$, which is still under discussion in the literature, see ref. [11] and references therein. Also, the nucleon polarizabilities manifest themselves in a different way in γn and γp scattering. The corresponding low-energy structure correction to the differential cross section is proportional to E_γ^4 in the case of neutron and to E_γ^2 for the proton [10, 12].

Nowadays, the interest in measuring the electric (α) and magnetic (β) polarizabilities of stable hadrons such as N, π, K, Σ is noticeably increasing due to understanding of their significance for selecting realistic constituent and quantum-field models of nonperturbative QCD, see, e.g., refs. [12–18]. Until recently, only polarizabilities of the proton and charged pion have been measured. For a long time the attempts to determine the neutron electric polarizability α_n in experiments on low-energy neutron scattering by heavy nuclei, i.e. to reveal the polarization interaction $V^{\rm pol} = -\frac{1}{2}\alpha_n \mathbf{E}^2$ of the neutron with the nuclear Coulomb field $\mathbf{E}$, were unsuccessful. The troubles were in precisely measuring the neutron-scattering cross sections and, second, in reducing uncertainties in the background caused by the strong neutron-nucleus interaction. The upper limits found in earlier experiments, e.g. $|\alpha_n| \leqslant 60$ in ref. [2], were essentially higher than the theoretical estimate [12]

$$\alpha_n \simeq 11 \pm 3, \tag{3}$$

based on dispersion sum rules. Only recently, very precise measurements [3–5, 19] of the neutron transmission cross section of Pb and Bi have been performed, and the best data by the Vienna-Oak Ridge group for the pure isotope ^{208}Pb [19] resulted in the following value of the neutron polarizability

$$\alpha_{0n}^{\rm exp} = 12.0 \pm 1.5\,(\text{stat}) \pm 2.0\,(\text{syst}). \tag{4}$$

Note that the so-called static polarizability α_{0n} has been found in ref. [19]. To obtain the "generalized static" polarizability α_n relevant to the present and most other applications, a small relativistic correction $\Delta\alpha_n = 0.62$ must be added to α_{0n}, so that

$$\alpha_n^{\exp} = 12.6 \pm 1.5\,(\text{stat}) \pm 2.0\,(\text{syst}). \tag{5}$$

The value (5) is in agreement with Eq. (2) and the theoretical estimate (3) and is also close to the proton electric polarizability, $\alpha_p^{\exp} \simeq 11$ [20–24]. According to dispersion theory [12], a small difference $\alpha_n - \alpha_p \simeq 2$ can be expected as being due to the nucleon recoil while exciting the pionic cloud of the nucleon by a probe.

Calculations within the cloudy bag model [13] show that the contribution of the pion cloud to the nucleon electric polarizability α_N is more than that of the quark core, provided the core radius is $R_c \simeq 0.5$ to 0.6 fm, what is necessary to have, e.g., a realistic excitation spectrum of the core. The dominating role of pions in the electric polarizability α_N is supported also by calculations within the dispersion approach [25] and chiral perturbation theory [16]. However, all constituent models have difficulties with the description of the paramagnetic and diamagnetic parts of β_N, see, e.g., ref. [18]. Further, more accurate measurements of the nucleon polarizabilities in experiments on γn and γp scattering below the pion threshold could shed more light on the relative role of quark and mesonic degrees of freedom in the nucleon structure at intermediate range, where the predictive abilities of QCD are limited.

Recently, uncertainties related to the strong neutron-nucleus interaction were suspected [26] as being underestimated in refs. [3, 4, 19] when α_n was extracted from nA scattering data. So, further more accurate studies of γn scattering are worth pursuing to get independent information on α_n.

Further investigations of γn scattering are desirable also for other reasons. We mean here that the detailed knowledge of γn and γp scattering amplitudes is needed for a consistent interpretation of data on photon scattering by nuclei and for studies of bound nucleons and meson-exchange currents as seen in two-photon reactions.

In principle, γn scattering could be studied by the method used already for $\gamma\pi^-$ scattering [27, 28], i.e. through the Primakoff effect in the radiative scattering of multi-GeV neutrons by nuclei [29]. Such a way, however, is hardly feasible at the moment because it needs a high-collimated intense neutron beam. A more natural possibility to obtain data on γn scattering is provided by the reaction (1). If the proton gets in this reaction a small momentum $\mathbf{p}_p$ and hence is a spectator, the reaction amplitude is dominated by the neutron pole diagram. Correspondingly, the differential cross section $d^4\sigma/d\Omega_\gamma\, d^3\mathbf{p}_p$ has a peak at small $\mathbf{p}_p$ (this is the neutron quasi-free peak, NQFP) and, in the peak region, is essentially proportional to the differential cross section of γn scattering [7].

In the present paper we extend the calculations of our earlier work [7]. We include now the np rescattering in the final state in P- and D-waves, apart from the previously considered S-wave rescattering. Also, the realistic NN potential (Paris) [30, 31] is used for finding the rescattering T-matrix. We consider corrections due to meson-exchange and isobar currents (MEC and IC) as well and evaluate them by using the Blomqvist-Laget model of the photo-pion reactions on nucleons [32]. Generally, the diagrammatic method used here to take into account the final-state interaction, MEC, and IC works successfully in many applications to the processes $\gamma d \to np$, $\gamma d \to \pi NN$, etc. [33, 34].

While evaluating individual diagrams, realistic on-shell γN scattering amplitudes are used instead of the blocks with two photon and two nucleon external lines. Such amplitudes have been calculated at $E_\gamma \lesssim 400$ MeV with the help of relativistic

finite-energy dispersion relations [10]. The amplitudes depend on one free or, at least, poorly known parameter linearly related with the difference of the nucleon polarizabilities $\alpha_N - \beta_N$, which thereby becomes the aim of fitting the experimental data. At the same time, the sum of the polarizabilities, $\alpha_N + \beta_N$, is not varied because it is calculated rather reliably in dispersion theory [12]:

$$\alpha_n + \beta_n \simeq 15.8 \pm 0.5, \qquad \alpha_p + \beta_p \simeq 14.2 \pm 0.5. \tag{6}$$

The content of the present paper is as follows. The main kinematic relations and general formulae are introduced in Sect. 2. In Sects. 3–5, the contributions of individual diagrams to the amplitude of the reaction (1) are discussed. The numerical results are presented in Sect. 6, Sect. 7 is devoted to concluding remarks.

2 Kinematics

We discuss here the kinematics of the reaction (1) for the case of the deuteron being at rest and keeping in mind the following applications to the quasi-free γn scattering in which the proton has a small momentum and is not detected under usual experimental conditions. We denote by p_γ, p_d, $p_{\gamma'}$, p_n and p_p the 4-momenta of the initial and final particles of the reaction (1). The energy-momentum conservation,

$$E_\gamma + E_d = E_{\gamma'} + E_p + E_n, \qquad \mathbf{p}_\gamma = \mathbf{p}_{\gamma'} + \mathbf{p}_p + \mathbf{p}_n, \tag{7}$$

where E_N are nucleon kinetic energies and $-E_d = \Delta = 2.2246$ MeV is the deuteron binding energy, enables one to determine the momentum of the spectator proton provided both directions of the scattered photon ($\theta_{\gamma'}$, $\phi_{\gamma'}$) and neutron (θ_n, ϕ_n) and two of three energies E_γ, $E_{\gamma'}$ and E_n are known. For example, by measuring the energies of the final photon and neutron and their angles, one can find the initial photon energy from Eq. (7) as

$$E_\gamma = \frac{E_{\gamma'}(m - \Delta - E_n + |\mathbf{p}_n| \cos\theta_{\gamma' n}) + (2m - \Delta)(E_n + \frac{1}{2}\Delta)}{m - \Delta - E_n + |\mathbf{p}_n| \cos\theta_n - E_{\gamma'}(1 - \cos\theta_{\gamma'})}. \tag{8}$$

Here $\theta_{\gamma' n}$ is the angle between $\mathbf{p}_{\gamma'}$ and $\mathbf{p}_n$, m is the nucleon mass, and the polar z-axis is chosen along the initial photon beam. Then the proton momentum is reconstructed through relation (7). Similarly one finds $E_{\gamma'}$ if the energy E_γ is known, e.g., due to the use of tagged photons.

We shall further see that the contribution to the reaction amplitude from the subprocess of γn scattering depends on E_p as $\propto (2E_p + \Delta)^{-1}$, thus resulting in a peak at small E_p in the differential cross section, which is clearly seen if $E_n \gg \Delta$. The region of the NQFP is qualitatively characterized by the condition

$$E_p \lesssim \tfrac{1}{2}\Delta \simeq 1.1 \text{ MeV}. \tag{9}$$

In the centre of the NQFP, i.e. at $E_p = 0$, the 3-momenta of all particles lie in the same plane and their energies and angles are given by the equations

$$E_n^{\text{peak}} = \frac{E_\gamma(E_\gamma - \Delta)(1 - \cos\theta_{\gamma'}) + \frac{1}{2}\Delta^2}{m - \Delta + E_\gamma(1 - \cos\theta_{\gamma'})}, \tag{10}$$

$$E_{\gamma'}^{\text{peak}} = E_\gamma - E_n^{\text{peak}} - \Delta, \tag{11}$$

$$\tan \theta_n^{\text{peak}} = \frac{-\sin \theta_{\gamma'} E_{\gamma'}^{\text{peak}}}{E_\gamma - \cos \theta_{\gamma'} E_{\gamma'}^{\text{peak}}}, \tag{12}$$

which coincide with the corresponding formulae for photon scattering by a free nucleon at rest in the limit of $\Delta = 0$. The relations (9)–(12) determine the kinematic region of the reaction (1) which has to be covered by any experimental setup aiming at the investigation of γn scattering at the energy E_γ and angle $\theta_{\gamma'}$ chosen. Loosely speaking, the neutron momentum $\mathbf{p}_n$ should lie within the sphere of the radius $|\Delta \mathbf{p}_n| \simeq \alpha = \sqrt{m\Delta} \simeq 45.7$ MeV and centered at $\mathbf{p}_n^{\text{peak}}$ with the appropriate energy (10) belonging to the region of the NQFP.

In terms of the reaction amplitude T_{fi},

$$S_{fi} = -i(2\pi)^4 \delta^{(4)}(p_\gamma + p_d - p_{\gamma'} - p_n - p_p) \sqrt{\frac{1}{4E_\gamma E_{\gamma'}} \frac{m^2}{\varepsilon_p \varepsilon_n}}\, T_{fi} \tag{13}$$

with the states normalized as $\langle \mathbf{p}' | \mathbf{p} \rangle = (2\pi)^3 \delta^{(3)}(\mathbf{p}' - \mathbf{p})$ and $\varepsilon_N = E_N + m$ being the nucleon total energy, the laboratory (lab) differential cross section of the reaction (1) reads

$$\frac{d^3\sigma}{d\Omega_{\gamma'}\, d\Omega_n\, dE_n} = \frac{m|\mathbf{p}_n| E_{\gamma'}^2}{4E_\gamma E_{\gamma'}^{(p)}} \frac{|T_{fi}|^2}{(2\pi)^5}, \tag{14}$$

where $E_{\gamma'}^{(p)} = (p_{\gamma'} p_p)/m$ is the energy of γ' in the proton rest frame. In Eq. (14) the usual sum and average over final and initial polarizations is implied.

Another observable we shall consider can be measured if a linearly-polarized γ-beam is available. This is the cross-section asymmetry for parallel and perpendicular polarizations of initial photons with respect to a chosen azimuthal xz-plane, which can, e.g., be the azimuthal plane of the outgoing photon or neutron. The asymmetry is determined by the interference of amplitudes $T_{fi}(\lambda)$ with opposite helicities λ of initial photons,

$$\Sigma = \frac{d\sigma_\perp - d\sigma_\parallel}{d\sigma_\perp + d\sigma_\parallel} = \frac{2\,\mathrm{Re}[T_{fi}(\lambda = 1) T_{fi}^*(\lambda = -1)]}{|T_{fi}(\lambda = 1)|^2 + |T_{fi}(\lambda = -1)|^2}. \tag{15}$$

Here the sum over polarizations of d, γ', n, and p is implied and the relative phase of the polarization vectors $\mathbf{e}_\lambda$ of γ with helicities $\lambda = 1$ and $\lambda = -1$ is fixed by

$$\mathbf{e}_\lambda = -\frac{1}{\sqrt{2}}(\lambda \hat{\mathbf{x}} + i\hat{\mathbf{y}}). \tag{16}$$

Since in the following numerical calculations we shall consider only on-plane kinematics, which covers the centre of the NQFP and has coincident $\gamma\gamma'$- and γn-planes, we make no distinction between the corresponding $\Sigma_{\gamma'}$ and Σ_n asymmetries and denote the asymmetry simply by Σ.

3 Pole Diagrams

We use the diagrammatic approach to calculate the amplitude T_{fi}. According to this method, the amplitude of the process is approximated by a few dominating diagrams, which have singularities close to the physical region of kinematic variables, see, e.g., refs. [8, 9].

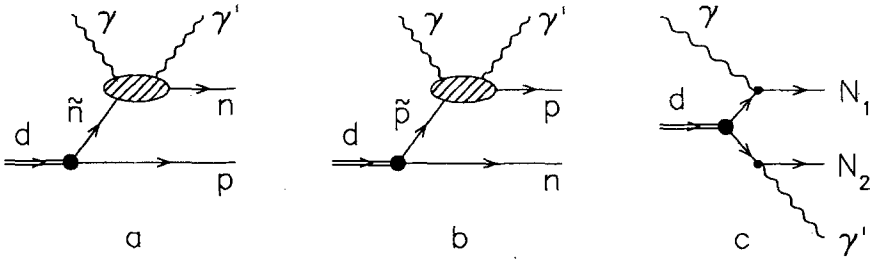

Fig. 1. Pole diagrams for the reaction $\gamma d \to \gamma' np$

We begin with discussion of the pole diagrams. Since we aim to extract information on the γn scattering amplitude, we should first take into account the contribution of the diagram in Fig. 1 a and choose the kinematics in which this diagram dominates. Using Feynman rules for nuclear reactions [8], we write down the corresponding amplitude as

$$T_{fi}^{1a} = \langle \gamma' n | T | \gamma \tilde{n} \rangle \frac{1}{E_d - E_p - E_{\tilde{n}}} \Gamma_{p\tilde{n}}^d(\mathbf{p}_p) = \langle \gamma' n | T | \gamma \tilde{n} \rangle \psi_{p\tilde{n}}^d(\mathbf{p}_p), \tag{17}$$

where $\Gamma_{p\tilde{n}}^d(\mathbf{p}_p)$ is the vertex of the $d \to p\tilde{n}$ transition,

$$\psi_{p\tilde{n}}^d(\mathbf{p}_p) = \frac{1}{E_d - E_p - E_{\tilde{n}}} \Gamma_{p\tilde{n}}^d(\mathbf{p}_p) \tag{18}$$

is the deuteron wave function, and $\langle \gamma' n | T | \gamma \tilde{n} \rangle$ is the half-off-shell γn scattering amplitude. We imply but do not indicate explicitly here and below the summation over spin indices of intermediate particles. Since the nucleon propagator in Eq. (17) is

$$\frac{1}{E_d - E_p - E_{\tilde{n}}} = -\frac{1}{2E_p + \Delta} \simeq -\frac{m}{\mathbf{p}_p^2 + \alpha^2}, \tag{19}$$

the diagram in Fig. 1 a has a pole singularity in E_p located at the point $E_p = -\Delta/2 \simeq -1.1$ MeV. When the proton-spectator momentum $|\mathbf{p}_p| \to 0$, we approach this singularity closely, and the contribution of Fig. 1 a is maximal. The region of $|\mathbf{p}_p| \lesssim \alpha$ is just the region of the NQFP.

Let us introduce the cross section of the $\gamma\tilde{n} \to \gamma' n$ process in the deuteron rest frame, in which the intermediate (almost on-shell) neutron $\tilde{n}$ is moving:

$$\frac{d\sigma(\gamma\tilde{n} \to \gamma' n)}{d\Omega_{\gamma'}} = \frac{m}{v\varepsilon_{\tilde{n}}} \frac{E_{\gamma'}^2}{E_\gamma E_{\gamma'}^{(n)}} \frac{|\langle \gamma' n | T | \gamma \tilde{n} \rangle|^2}{(4\pi)^2}. \tag{20}$$

Here $E_{\gamma'}^{(n)} = (p_{\gamma'} p_n)/m$ is the energy of γ' in the neutron n rest frame and $v = 1 - p_{\tilde{n}z}/p_{\tilde{n}0}$ is the relative velocity of initial photon and neutron $\tilde{n}$. Then the differential cross section of the reaction (1) with the amplitude (17) is recast into

$$\frac{d^4\sigma^{1a}}{d\Omega_{\gamma'}\, d^3\mathbf{p}_p} = v \frac{|\psi_{p\tilde{n}}^d(\mathbf{p}_p)|^2}{(2\pi)^3} \frac{d\sigma(\gamma\tilde{n} \to \gamma' n)}{d\Omega_{\gamma'}} \tag{21}$$

and has a simple interpretation: It is the differential cross section of the "elementary" subprocess $\gamma\tilde{n} \to \gamma' n$ times the probability to find the spectator p with the momentum $\mathbf{p}_p$ inside the deuteron times the flux factor v due to the movement of the neutron

$\tilde{n}$. Another form of expression (21) is given by

$$\frac{d^3\sigma^{1a}}{d\Omega_{\gamma'}\, d\Omega_n\, dE_n} = v\frac{|\psi^d_{p\tilde{n}}(\mathbf{p}_p)|^2}{(2\pi)^3}\frac{|\mathbf{p}_n|\varepsilon_p E^{(n)}_{\gamma'}}{E^{(p)}_{\gamma'}}\frac{d\sigma(\gamma\tilde{n}\to\gamma' n)}{d\Omega_{\gamma'}}. \tag{22}$$

These formulae can be used to extract the γn scattering cross section from measurements of $d^3\sigma/d\Omega_{\gamma'}\, d\Omega_n\, dE_n$ provided the contributions from other diagrams and off-shell corrections are small or taken into account, or an extrapolation in E_p is made, see Sect. 6.

Apart from the mechanism represented by Fig. 1 a, a similar process is possible with the photon scattered by the proton, see Fig. 1 b. The corresponding amplitude is

$$T^{1b}_{fi} = \langle\gamma' p|T|\gamma\tilde{p}\rangle\frac{1}{E_d - E_n - E_{\tilde{p}}}\Gamma^d_{\tilde{p}n}(\mathbf{p}_n) = \langle\gamma' p|T|\gamma\tilde{p}\rangle\psi^d_{\tilde{p}n}(\mathbf{p}_n); \tag{23}$$

it also has a pole singularity $\propto (2E_n + \Delta)^{-1}$. If we want the contribution from Fig. 1 b to be suppressed, we should choose the kinematics with $E_n \gg \Delta$. According to Eq. (10), it takes place if the photon is scattered at not too small an angle. In the following we shall consider just such kinematics. Note that particularly the large-angle amplitude of $\gamma\tilde{n}\to\gamma' n$ is most sensitive to the difference $\alpha_n - \beta_n$ of the neutron polarizabilities and to the sign of $F_{\pi^0\gamma\gamma}$ [10].

Evaluation of the amplitudes (17) and (23) requires knowing the deuteron wave function ψ^d_{pn}, which is specified in the next section, and the half-off-shell nucleon Compton scattering amplitude $\langle\gamma' N|T|\gamma\tilde{N}\rangle$. For a free nucleon, a realistic γN scattering amplitude is provided by dispersion relations. It is not possible to use the same dispersion technique for a bound nucleon because of the lack of appropriate photoproduction input. On the other hand, simple diagrammatic models of Blomqvist-Laget type, which are very suitable for off-shell extrapolations and based on tree diagrams of γN-scattering plus the Δ-isobar contribution, are too rough for on-shell nucleons, see, e.g., the discussion in ref. [25]. So, we have preferred here to rely on the dispersion calculations of ref. [10], which are rather accurate for a free nucleon. Although, thereby, we essentially neglected the nucleon off-shell effects; note that the neutron $\tilde{n}$ is off the energy shell only by $\lesssim$2–4 MeV in the kinematic region of the NQFP. For Fig. 1 b, the off-shell shift of $\tilde{p}$ is higher but the whole contribution of the amplitude (23) is very small, see Sect. 6.

The on-shell Compton scattering amplitude is described by six complex functions $R_i(W, \theta^*)$ of the total centre-of-mass (c.m.) energy W and c.m. scattering angle θ^* [12]. It reads, in the c.m. frame, as

$$\begin{aligned}
\langle\lambda', \pm\tfrac{1}{2}|T|\lambda, \pm\tfrac{1}{2}\rangle &= 4\pi\frac{W}{m}\frac{1+\lambda\lambda' z}{2}[-(R_1 + \lambda\lambda' R_2) \pm (\lambda R_3 + \lambda' R_4) \\
&\quad \pm (1+\lambda\lambda' z)(\lambda' R_5 + \lambda R_6)], \\
\langle\lambda', \mp\tfrac{1}{2}|T|\lambda, \pm\tfrac{1}{2}\rangle &= 4\pi\frac{W}{m}\sin\theta^*\left[\frac{1+\lambda\lambda' z}{2}(\lambda R_5 + \lambda' R_6)\right. \\
&\quad \left. + \frac{1\mp\lambda}{2}(\lambda' R_3 + \lambda R_4)\right],
\end{aligned} \tag{24}$$

where $z = \cos\theta^*$, λ and λ' are photon helicities, and $\pm\frac{1}{2}$ indicates the nucleon spin

projections on the direction of γ in the c.m. frame. We have used the same on-shell formulae as a substitute for the off-shell amplitude $\langle\gamma' N|T|\gamma\tilde{N}\rangle$. More specifically, the Compton amplitudes in Eqs. (17) and (23) have been substituted by the right-hand sides of Eq. (24) found at the total energy $W = \sqrt{(p_{\gamma'} + p_N)^2}$ and the scattering angle $\theta^* = \theta^*_{\gamma'}$ in the c.m. frame of the $\gamma' N$ pair.

It is easy to understand that in Eq. (24) the use of the same energy W as in the subprocess of Compton scattering off a virtual nucleon is essential to take properly into account the strong energy dependence of the Compton amplitude due to Δ-resonance excitation. The choice $\theta^* = \theta^*_{\gamma'}$ is not so crucial but it keeps in the same regime angular factors of most important diagrams of γN-scattering, i.e. Δ-excitation (both for p and n) and Thomson term (for p). By studying a simple diagrammatic model with spinless point-like deuteron and nucleons, we have observed that the prescription used to substitute W and θ^* ensures a high accuracy of $\lesssim 1\%$ for the amplitude T_{fi} in the NQFP region.

The amplitudes R_i in Eq. (24) carry information on the nucleon polarizabilities used. In the limit of $\omega \equiv (W^2 - m^2)/2m \to 0$, all the $R_i(W, \theta^*)$ are equal to zero except

$$R_1 = -\frac{e^2}{4\pi m}\frac{1+\tau_3}{2} + O(\omega). \tag{25}$$

The electric and magnetic nucleon polarizabilities manifest themselves in the quadratic low-energy corrections to the amplitudes R_1 and R_2:

$$R_1^{\text{pol}} = \omega^2 \alpha_N + O(\omega^3), \qquad R_2^{\text{pol}} = \omega^2 \beta_N + O(\omega^3). \tag{26}$$

The amplitudes R_5 and R_6 incorporate the π^0-exchange contribution,

$$R_5^{\pi^0} = -R_6^{\pi^0} = \frac{m^3\omega^3}{8\pi W^4}\frac{g_{\pi NN}F_{\pi^0\gamma\gamma}}{t - m_{\pi^0}^2}\tau_3, \qquad t = (p_{\gamma'} - p_\gamma)^2, \tag{27}$$

which depend on the magnitudes and relative sign of the πNN and $\pi^0\gamma\gamma$ couplings. Numerical values of the amplitudes R_i are borrowed from the dispersion calculations of ref. [10].

Since the polarizability of the neutron appears in the total Compton scattering amplitude together with other contributions, which are typically greater than those of Eq. (26), the important question arises whether it is possible to determine α_n accurately on the background of those contributions estimated theoretically. In part, this question was already analyzed in ref. [10] and now we update these previous findings. In the region of low energies, $E_\gamma \sim 100$ MeV, the most important uncertainty in the γn scattering amplitude turns out to be related with the coupling constants $g_{\pi NN}$ and $F_{\pi\gamma\gamma}$ of the t-channel π^0-exchange. There is some controversy about both of them, see, e.g., refs. [35–37], and the product $g_{\pi NN}F_{\pi\gamma\gamma}$ is presently known to within $\pm 5\%$. Together with uncertainties in the Δ-resonance tail, etc. this leads to 1–2% variations in theoretical cross sections (depending on energies and angles) and prevents to determine α_n better than $\sim \pm 2$, provided α_n is close to the value of 12 as given by the nA experiment [19].

At higher energies, $E_\gamma \sim 250$ MeV, the uncertainties in the theoretical γn scattering amplitude are mostly stemming from the absolute normalization of the Δ-excitation amplitude. At the moment, the total theoretical uncertainties in the

predicted γn scattering cross section are estimated to be $\approx 10\%$, as seen from the variances between different partial-wave analyses of single-pion photoproduction off neutron in the Δ-resonance region used as input for the dispersion calculations [38–41]. In principle, the correct normalization of the Δ-excitation can be established by measuring the same γn scattering (through the reaction $\gamma d \to \gamma' np$) very near the Δ-peak, and the remaining uncertainty in the cross section is $\approx 5\%$. So, with the normalization uncertainty fixed, the uncertainty in the extracted value of α_n from data at $E_\gamma \sim 250$ MeV related with the dispersion model of Compton scattering can be reduced to $\simeq \pm 2$.

Eqs. (17) and (23) are written down in the deuteron rest frame and hence contain the amplitudes $\langle \gamma' N | T | \gamma \tilde{N} \rangle$ in that frame, whereas the formulae (24) are valid with the nucleon spin projections taken in the c.m. frame of the $\gamma' N$-pair. Therefore, it would be more appropriate to combine the expressions (24) with relativistic rotations of nucleon spins [46] (note that the photon helicities are Lorentz invariant) to take into account the difference between the lab and $\gamma' N$ frames. We have neglected such rotations on the basis of the following arguments. The effect of the spin rotations vanishes in the dominating contribution (22) to the cross section, as well as in the much smaller contribution of Fig. 1 b, because there the quantity $|\langle \gamma' N | T | \gamma \tilde{N} \rangle|^2$ is Lorentz invariant and can be evaluated in any frame. The contributions due to interference of Figs. 1 a and 1 b and *np* rescattering do depend on the spin rotations but they are too small in total to make the relativistic effects of the order of $(\omega/m)^2$ noticeable in the cross section. In whole, the semi-relativistic procedure used to evaluate the pole diagrams in the NQFP region has the merit of being exact at high energies when the contribution (21) survives alone.

Another type of pole diagrams is shown in Fig. 1 c. It is easy to establish that the corresponding amplitude is suppressed, as compared to the one of the diagram in Fig. 1 a, at least by the factor of Δ/E_γ, which is $\lesssim 0.02$ in the kinematics considered. Only at energies below ~ 50 MeV the contribution of Fig. 1 c becomes noticeable. We neglect it in the present paper.

4 One-Loop Diagrams with *np* Rescattering

Within the diagrammatic approach studies of various processes with deuteron break-up, such as $\gamma d \to np$, $ed \to enp$, $\gamma d \to \pi NN$ [9, 33, 34], show that diagrams with the nucleon rescattering noticeably contribute to the reaction amplitude. In the case of the two-photon reaction (1), the rescattering can take place both in the final and intermediate state, see the diagrams in Fig. 2, which exhaust the rescattering corrections in the one-loop approximation.

Let us discuss first the diagram in Fig. 2 a with photon scattering by a proton or neutron. In the processes of $2 \to 3$ type, including the reaction $\gamma d \to \gamma' np$, the relative scale of the contributions to T_{fi} from the triangle and pole diagrams is very different, depending on energies and angles [8]. The location of the triangle singularity t_s of Fig. 2 a in the variable $t = (p_{\gamma'} - p_\gamma)^2$ depends on the energy E_{np} of relative motion of the nucleons *n* and *p*. The value of t_s is $4\alpha^2$ if $E_{np} = 0$ and thus it is very close to the physical region. Therefore, for small-angle photon scattering and small E_{np}, Fig. 2 a is very important. Even with increasing photon scattering angle, the contribution T_{fi}^{2a} remains noticeable, especially at low photon energies $\lesssim 100$ MeV,

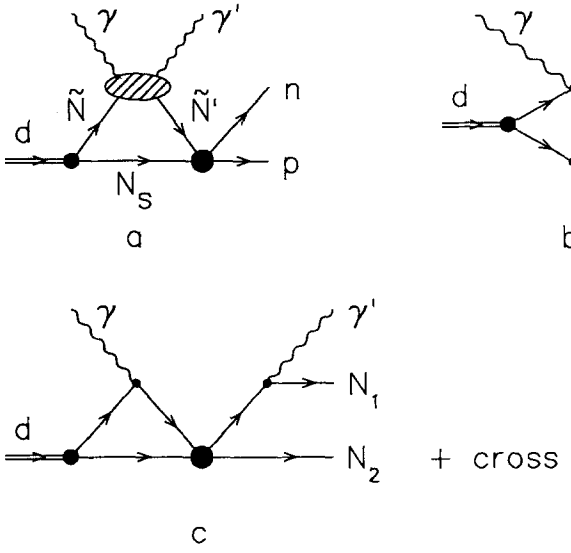

Fig. 2. One-loop diagrams with *np* rescattering in the final (**a**, **b**) and intermediate (**c**) state

because then the energy E_{np} is also not high, being, e.g., ~ 7 MeV at $E_\gamma = 100$ MeV and $\theta_{\gamma'} = 135°$ in the NQFP region, and the *S*-wave *np* scattering is rather strong.

On the contrary, the contribution T_{fi}^{2b} of Fig. 2 b is less essential. Since again the *S*-wave plays the leading role in the *np* rescattering, essentially magnetic-type couplings in the γNN vertex contribute to the amplitude T_{fi}^{2b}. As a result, T_{fi}^{2b} proves to be suppressed by the factor of E_γ/m as compared with the amplitude T_{fi}^{2a} of γp scattering and it is of the same order as the contribution of Fig. 1 c. Numerically, Fig. 2 a contributes $\sim -30\%$ at $E_\gamma = 100$ MeV and $\sim -7\%$ at $E_\gamma = 400$ MeV to the cross section in the NQFP region, so the contribution T_{fi}^{2b} can be safely neglected.

One can see in a similar way that the contribution T_{fi}^{2c} of Fig. 2 c with rescattering in the intermediate state is suppressed like E_γ/m in comparison with T_{fi}^{2a} and hence it is not important. The smallness of the contribution like T_{fi}^{2c} with respect to T_{fi}^{2a} has been emphasized also by Weyrauch [47] in his studies of elastic γd scattering; in the elastic case, however, there are no pole diagrams (Figs. 1 a–1 b) and the rescattering in the intermediate state is more essential in total: It is at the level of 10% at $E_\gamma \sim 50$–100 MeV in the forward-angle cross section, and $\lesssim 3\%$ when $\theta_{\gamma'} \geqslant 90°$ [47].

Thus, we keep only the diagram in Fig. 2 a for numerical calculations. The corresponding contribution reads

$$T_{fi}^{2a} = m \int \frac{d^3\mathbf{p}_{N_S}}{(2\pi)^3} \frac{\langle np|\, T(E_{np})\,|\tilde{N}'N_S\rangle \langle \gamma'\tilde{N}'|\, T\,|\gamma\tilde{N}\rangle}{\mathbf{q}^2 - \tilde{\mathbf{q}}^2 + i0} \psi^d_{\tilde{N}N_S}(\mathbf{p}_{N_S}), \tag{28}$$

where $\tilde{\mathbf{q}} = \mathbf{p}_{N_S} - \frac{1}{2}(\mathbf{p}_\gamma - \mathbf{p}_{\gamma'})$ and $\mathbf{q} = \frac{1}{2}(\mathbf{p}_p - \mathbf{p}_n)$ are relative c.m. momenta of the *np* pair before and after the rescattering, respectively, and $\langle np|\, T(E_{np})\,|\tilde{N}'N_S\rangle$ is the half-off-shell *np* scattering amplitude at the energy $E_{np} = \mathbf{q}^2/m \neq \tilde{\mathbf{q}}^2/m$. The sum over $\tilde{N} = p, n$ is implied in Eq. (28).

The energy W at which the amplitude $\langle \gamma'\tilde{N}'|\, T\,|\gamma\tilde{N}\rangle$ has to be used in the integrand of Eq. (28) should be specified too. Considering, in accordance with ref.

[9], Fig. 2 a in the Feynman formalism with 4-momenta conservation and additional loop integration over the energy, we neglect singularities at energies $\sim 2m$ and close the integration contour around the nearest pole of the propagator of the nucleon-spectator N_S. Then we arrive just at the formula (28) with the nucleon N_S being on mass-shell. Accordingly, we calculate the energy W in the vertex $\langle \gamma' \tilde{N}' | T | \gamma \tilde{N} \rangle$ by using the nucleon $\tilde{N}$ energy $p_{\tilde{N}0} = 2m - \Delta - \sqrt{\mathbf{p}_{N_S}^2 + m^2}$ and momentum $-\mathbf{p}_{N_S}$.

The integral in Eq. (28) receives contributions mainly at low momenta $|\mathbf{p}_{N_S}| \sim \alpha$ when the deuteron wave function is not too small. For this reason the nucleon $\tilde{N}$ is effectively off the energy shell by only a few binding energies Δ. Moreover, just in the kinematics of quasi-free Compton scattering, the intermediate recoil nucleon $\tilde{N}'$ will also be near the energy shell whenever the initial nucleon $\tilde{N}$ is almost at rest and on shell. So, both Compton scattering and rescattering blocks appear in Eq. (28) effectively in a near-on-shell regime and off-shell corrections are expected to be small.

For getting a more quantitative estimate of the importance of higher momenta $\mathbf{p}_{N_S}$, we introduced into Eq. (28) the form factor $\Lambda^2/(\Lambda^2 + p_{N_S}^2)$ with $\Lambda = 200$ MeV and we observed that in three typical quasi-free kinematics, namely at $E_\gamma = 100$, 250, and 400 MeV with $\theta_{\gamma'} = 135°$, the change in the resulting cross section (14) was $+4\%$, -2.5% and -1.5%, respectively.

Since the nucleon $\tilde{N}'$ is effectively near the energy shell, various NN potentials are expected to give very similar half-off-shell scattering amplitudes. Such a feature was explicitly demonstrated for the Paris and Reid soft-core potentials in ref. [42] and a similar comparison for the Paris and three versions of the Bonn potential was done in ref. [43]. In the following, for getting the deuteron wave function and the np rescattering amplitude we shall use the Paris potential [30] in the separable approximation of ref. [31], which is convenient for us because it directly provides these quantities in the momentum space.

The deuteron wave function is

$$\psi_{pn}^{d}(\mathbf{q}) = \psi_{np}^{d}(\mathbf{q}) \equiv \psi_{m_p m_n}^{m_d}(\mathbf{q})$$

$$= \frac{1}{\sqrt{4\pi}} C_{(1/2)m_p(1/2)m_n}^{1 m_d} u(q) - C_{(1/2)m_p(1/2)m_n}^{1 m_S} C_{2 m_L 1 m_S}^{1 m_d} Y_{2 m_L}(\hat{\mathbf{q}}) w(q), \qquad (29)$$

where $m_p, m_n, m_d, m_S = m_p + m_n$ and $m_L = m_d - m_S$ denote z-projections of the spins of the particles, of the total spin and orbital angular momentum; $Y_{Lm_L}(\hat{\mathbf{q}})$ are spherical harmonics. It is normalized as

$$\int \frac{d^3\mathbf{q}}{(2\pi)^3} |\psi_{pn}^{d}(\mathbf{q})|^2 \equiv \frac{1}{3} \sum_{m_p m_n m_d} \int \frac{d^3\mathbf{q}}{(2\pi)^3} |\psi_{m_p m_n}^{m_d}(\mathbf{q})|^2 = \int_0^\infty \frac{q^2\, dq}{(2\pi)^3} [u^2(q) + w^2(q)]$$

$$= 1. \qquad (30)$$

The functions $u(q)$ and $w(q)$ are expressed in terms of (non-normalized) partial vertices [31]

$$g_i^{JLS}(q) = \langle JLSq | V_{NN} | E_i J(L) S \rangle \simeq \sum_{n=1}^{4} \frac{C_{in}^{JLS} q^{L+2(n-1)}}{[q^2 + (\beta_{in}^{JLS})^2]^{L-[L/2]+n}}. \qquad (31)$$

Here $|JLSq\rangle$ means the partial wave of the free particles at the relative momentum q, and $|E_i J(L) S\rangle$ is the eigenstate of the Paris potential V_{NN} in the np channel with

the energy E_i and quantum numbers $J(L)S$, where we use the generic symbol (L) to specify both uncoupled partial waves and those with mixed orbital momenta $L = J \pm 1$. These eigenstates compose the truncated basis of the separable expansion. The sum in Eq. (31) is a compact analytical representation of the functions $g_i^{JLS}(q)$. It is given in terms of the parameters C_{in}^{JLS} and β_{in}^{JLS} listed in ref. [31]. Since the deuteron is among the states $|E_iJ(L)S\rangle$ (that is the state $i = 1$ of the channel $^3S_1$-$^3D_1$ in the notations of ref. [31]), one can use Eq. (18) and write down

$$u(q) = -N\frac{m}{q^2+\alpha^2}g_{i=1}^{JLS}(q)|_{J=1,L=0,S=1}, \qquad w(q) = -N\frac{m}{q^2+\alpha^2}g_{i=1}^{JLS}(q)|_{J=1,L=2,S=1}. \tag{32}$$

Here the factor N provides the appropriate normalization (30) of the deuteron wave function; $N = 348.0\ \mathrm{MeV}^{3/2}$ for the PEST4 potential in ref. [31].

The off-shell amplitude of np scattering is also determined by the vertices g_i^{JLS},

$$\langle np|\,T(E)|\tilde{n}\tilde{p}\rangle = \sum_{JSL\tilde{L}m_Jm_Lm_Sm_{\tilde{L}}} C^{Sm_S}_{(1/2)m_p(1/2)m_n} C^{Sm_S}_{(1/2)\tilde{m}_p(1/2)\tilde{m}_n} C^{Jm_J}_{Lm_LSm_S} C^{Jm_J}_{\tilde{L}m_{\tilde{L}}Sm_S} \times (2\pi)^3 i^{\tilde{L}-L} Y_{Lm_L}(\hat{\mathbf{q}})(Y_{\tilde{L}m_{\tilde{L}}}(\hat{\tilde{\mathbf{q}}}))^* \langle JLSq|\,T(E)|J\tilde{L}S\tilde{q}\rangle, \tag{33}$$

where the partial np scattering amplitudes have the separable form

$$\langle JLSq|\,T(E)|J\tilde{L}S\tilde{q}\rangle = \sum_{i,j=1}^{R^{J(L)S}} g_i^{JLS}(q)\tau_{ij}^{J(L)S}(E)g_j^{J\tilde{L}S}(\tilde{q}), \qquad L, \tilde{L} \in (L). \tag{34}$$

Here $R^{J(L)S}$ is the number of eigenstates with different energies E_i included into the basis of the separable potential for the channel $J(L)S$. This is the rank of the separable potential. The matrix $\tau_{ij}^{J(L)S}(E)$ is determined, through its inverse, in terms of the matrix elements of the np potential,

$$\langle E_iJ(L)S|\,V_{NN}|E_jJ(L)S\rangle = [\lambda^{J(L)S}]_{ij}^{-1} \tag{35}$$

(the matrixes $\lambda_{ij}^{J(L)S}$ are also listed in ref. [31]), and the vertices g_i^{JLS}:

$$[\tau^{J(L)S}(E)]_{ij}^{-1} = [\lambda^{J(L)S}]_{ij}^{-1} - \sum_{L\in(L)} \int_0^\infty \frac{g_i^{JLS}(q)g_j^{JLS}(q)q^2\,dq}{E - \dfrac{q^2}{m} + i0}. \tag{36}$$

The related amplitude $\langle np|\,T(E)|\tilde{p}\tilde{n}\rangle$, which is needed to find the contribution to T_{fi}^{2a} of both proton and neutron Compton scattering, has the same form as expression (33) only with the replacement $\tilde{\mathbf{q}} \to -\tilde{\mathbf{q}}$ or, in other words, with the additional factor of $(-1)^{\tilde{L}}$ inside the sum in Eq. (33).

In our calculations of the amplitude T_{fi}^{2a} we take into account all partial waves considered in ref. [31], i.e. those with $(L) = (0), (1), (2)$; they include waves with $L = 3$, 4 coupled to the S-, P-, D-waves by tensor forces. The summation over polarizations in Eqs. (28) and (33) and the three-dimensional integration in Eq. (28) have been performed numerically.

Detailed discussion of calculations of the FSI correction with other potentials would bring us too far beyond the scope of the present paper. Here we give only a brief summary. Calculating the half-off-shell np rescattering T-matrix for the configuration space Bonn OBEPR (ref. [44], Table 14) and OBEP-A and OBEP-B potentials (ref. [45], Table A.3) we found that all versions of the Bonn potential

result in the same cross section (14) to within 1% (OBEP-A and OBEP-B giving the highest and lowest cross sections, respectively) in the above three typical kinematics of quasi-free scattering at 100, 250 and 400 MeV [43]. The Paris (PEST) potential gives systematically lower cross sections (by 3%, 1.4%, 1.8% at 100, 250, and 400 MeV, respectively). One may conclude that the uncertainties related with different forms of the NN potential are not large; however, they become more important in the case of low energies when the FSI correction is $\approx -30\%$.

5 One-Loop Diagrams with MEC and IC

The important role of subprocesses in which a meson is created at one nucleon and absorbed at another one is well known from many studies of form factors and photo- and electro-disintegration of few-nucleon systems. Owing to the small pion mass and the related large range, the one-pion component of the meson exchanges dominates at low momentum transfer, which is also the case for the reaction (1) in the NQFP region. In this section we calculate the pion-exchange contribution in one-loop approximation, see Fig. 3, which is justified provided $E_{np} \gg \Delta$; from studies of the reaction $\gamma d \to pn$ it is also known that corrections to the MEC + IC contribution due to np rescattering are typically small [34].

The amplitudes for Figs. 3 a and 3 b read

$$T_{fi}^{3a} = \int \frac{d^3\mathbf{p}_{\tilde{p}}}{(2\pi)^3} [\langle \gamma' p | T | \pi^0 \tilde{p} \rangle \langle \pi^0 n | T | \gamma \tilde{n} \rangle - \langle \gamma' n | T | \pi^- \tilde{p} \rangle \langle \pi^- p | T | \gamma \tilde{n} \rangle] \times \frac{\psi^d_{\tilde{p}\tilde{n}}(\mathbf{p}_{\tilde{p}})}{q^2 - m_\pi^2 + i0} + \left\{ \begin{array}{c} p \leftrightarrow n \\ \tilde{p} \leftrightarrow \tilde{n} \\ \pi^- \to \pi^+ \end{array} \right\} \tag{37}$$

and

$$T_{fi}^{3b} = -\frac{e^2 g_{\pi NN}^2}{m^2} (\mathbf{e}\mathbf{e}'^*) \int \frac{d^3\mathbf{p}_{\tilde{n}}}{(2\pi)^3} \frac{\langle p | (\boldsymbol{\sigma}\mathbf{q}_2) | \tilde{n} \rangle \langle n | (\boldsymbol{\sigma}\mathbf{q}_1) | \tilde{p} \rangle}{(q_1^2 - m_\pi^2 + i0)(q_2^2 - m_\pi^2 + i0)} \psi^d_{\tilde{p}\tilde{n}}(\mathbf{p}_{\tilde{n}}). \tag{38}$$

Here $\langle \pi N | T | \gamma \tilde{N} \rangle$ and $\langle \gamma' N | T | \pi \tilde{N} \rangle$ are the amplitudes of the pion photoproduction and the reverse reaction, respectively, and the nucleon brackets in Eq. (38) denote the corresponding nucleon spinors; $\mathbf{e}$ and $\mathbf{e}'$ are the photon polarization vectors; q, q_1 and q_2 are the pion 4-momenta, see Fig. 3; $g_{\pi NN}^2/4\pi = 14.5$.

Again the energies of the intermediate nucleons $\tilde{N}$ and $\tilde{N}'$ and pions have to be specified in Eqs. (37) and (38). Considering Fig. 3 a in the non-covariant perturbation

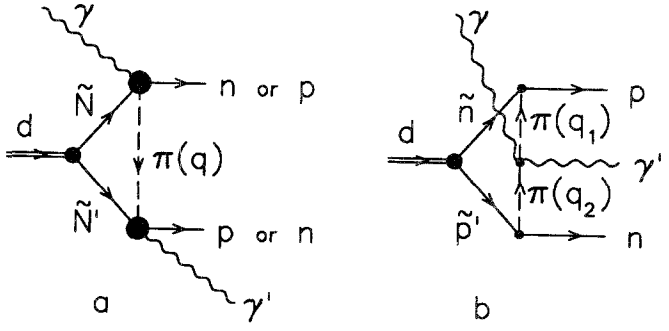

Fig. 3. One-loop diagrams with MEC and IC

theory, we would have two different sub-diagrams with opposite time-orderings of emitting and absorbing the pion. As was explained before, in each of these two sub-diagrams the energies in the corresponding $\gamma\pi NN$ vertices must be calculated as if the second nucleon was on the mass shell. The most essential energy factor appears in the sub-diagrams due to the non-covariant propagators which are, e.g.,

$$\frac{1}{E_\gamma + \varepsilon_d - \varepsilon_{\tilde{N}'} - \varepsilon_\pi - \varepsilon_n} + \frac{1}{-E_\gamma + \varepsilon_n - \varepsilon_{\tilde{N}} - \varepsilon_\pi} = \frac{1}{a - b - \varepsilon_\pi} - \frac{1}{a + b + \varepsilon_\pi}$$
$$= \frac{2(\varepsilon_\pi + b)}{(\varepsilon_\pi + b)^2 - a^2} \tag{39}$$

in the case of Fig. 3 a with $\gamma\pi\tilde{p}n$ vertex. Here the symbol ε denotes the total on-shell energies and

$$a = E_\gamma - \varepsilon_n + \tfrac{1}{2}(\varepsilon_d + \varepsilon_{\tilde{N}} - \varepsilon_{\tilde{N}'}) = E_\gamma - E_n - \tfrac{1}{2}\Delta,$$
$$2b = \varepsilon_{\tilde{N}'} + \varepsilon_{\tilde{N}} - \varepsilon_d = \frac{\tilde{\mathbf{p}}^2}{m} + \Delta. \tag{40}$$

It is reasonable to neglect the value of b in comparison with ε_π because b is effectively small in Fig. 3 a owing to the rapid vanishing of the deuteron wave function with increasing b. Then Eq. (39) becomes the relativistic pion propagator,

$$\frac{1}{\varepsilon_\pi^2 - a^2} = \frac{1}{m_\pi^2 + \mathbf{q}^2 - a^2}, \tag{41}$$

up to the factor $2\varepsilon_\pi$ that we shall include into the pion vertices.

Thus, the quantity a in Eq. (41), which is independent on the loop momentum $\tilde{\mathbf{p}}$, takes the role of the pion energy q_0 and is calculated as if the nucleons $\tilde{N}$ and $\tilde{N}'$ carried equal parts of the deuteron energy $\varepsilon_d = 2m - \Delta$. This rule of the equal off-shell shift of the nucleons will be used in evaluations of Eqs. (37) and (38).

The pion photoproduction amplitude $\langle \pi N | T | \gamma N \rangle$ in Eq. (37) has the form

$$\langle \pi N' | T | \gamma N \rangle$$
$$= ie_\pi \frac{g_{\pi NN}\sqrt{2}}{2m}\left[-\langle N' | (\boldsymbol{\sigma}\mathbf{e}) | N \rangle + 2(\mathbf{eq}) \frac{\langle N' | \boldsymbol{\sigma}(\mathbf{q} - \mathbf{p}_\gamma) | N \rangle}{(\mathbf{q} - \mathbf{p}_\gamma)^2 + m_\pi^2 - a^2 - i0} \right]$$
$$- i \frac{G_1 G_3}{2m} \sqrt{\tfrac{2}{3}} \lambda E_\gamma C_\pi \frac{\langle N' | \frac{2}{3}(\mathbf{eq}) + \frac{1}{3} i \boldsymbol{\sigma}(\mathbf{e} \times \mathbf{q}) | N \rangle}{E_\gamma + m - M_\Delta + \frac{1}{2} i \Gamma_\Delta}, \tag{42}$$

where $\mathbf{q}$ is the pion 3-momentum, e_π is the pion electric charge, λ is the photon helicity, and other parameters are specified below. The formula for the amplitude $\langle \gamma' N' | T | \pi N \rangle$ is obtained from Eq. (42) by Hermitean conjugation of all factors except $i0$ and $i\Gamma_\Delta$.

The first two terms in the right-hand side of Eq. (42) correspond to the diagrams a and b in Fig. 4. Together with T_{fi}^{3b}, they describe, after insertion into Eq. (37), the contribution of MEC to the amplitude T_{fi}. The last term in Eq. (42) is related to Δ-isobar excitation (Fig. 4 c) and determines the IC contribution to T_{fi}. The value C_π in this term is equal to $\mp\sqrt{\frac{1}{3}}$ for $\pi^\pm$-meson and $\sqrt{\frac{2}{3}}$ for π^0-meson. The $\gamma N\Delta$ and $\pi N\Delta$ couplings, G_1 and G_3, and the mass and width of the delta isobar are borrowed from the Blomqvist-Laget model [32],

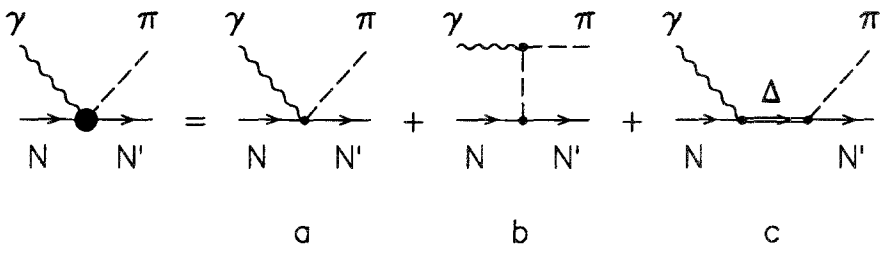

Fig. 4. Diagrammatic representation of the $\gamma N \to \pi N$ amplitude used

$$G_1 = 0.282 e_{\pi^+} \frac{M_\Delta + m}{m}, \qquad G_3 = \frac{2.18}{m_\pi}, \qquad M_\Delta = 1225 \text{ MeV},$$

$$\Gamma_\Delta(Q) = 110 \text{ MeV} \times \left(\frac{q(Q)}{q_\Delta}\right)^3 \frac{M_\Delta}{Q} \frac{1 + R^2 q_\Delta^2}{1 + R^2 q^2(Q)}, \tag{43}$$

where Q and $q(Q)$ are the total pion-nucleon energy and the corresponding pion momentum in their c.m. frame, $q_\Delta = q(M_\Delta) \simeq 220$ MeV and $R = 0.007$ MeV^{-1}.

Besides, the monopole form factor

$$F_\pi(q^2) = \frac{\Lambda_\pi^2 - m_\pi^2}{\Lambda_\pi^2 - q^2} \tag{44}$$

has been inserted into all pion-baryon vertices. The parameter $\Lambda_\pi = 1250$ MeV has been chosen consistently with the Paris potential [48]. However, we have observed that the variation of Λ_π within 50% did not produce any essential changes in the resulting cross sections, mainly because the contribution of MEC and IC is not very high itself.

Both the summation over polarizations of internal particles and the three-dimensional integrations in Eqs. (37)–(38) have been performed numerically.

In principle, the pion photoproduction amplitude (42) should include also the nucleon pole term. However, being kept in Eq. (37), the nucleon pole term produces some diagrams that are already included due to the use of initial and final eigenstates of the NN Hamiltonian incorporating one-pion exchange and hence they must be subtracted. Since, in the NQFP region, the contribution of MEC + IC turns out to be relatively small, the contribution of the nucleon pole term being even smaller, we preferred to simplify the consideration and omitted the nucleon pole term from the very beginning.

Of course, the nucleon pole term, being proportional to the nucleon 4-velocity, $p_\mu \varepsilon^\mu / m$, is small only in the transverse gauge

$$\varepsilon_0 = \boldsymbol{\varepsilon}\mathbf{k} = 0. \tag{45}$$

Though we have no manifestly gauge-invariant amplitude for MEC, by adhering to the approximation of no nucleon pole, which is justified in the specific gauge (45), we fix the gauge ambiguity.

The diagrammatic approach for calculations of MEC and IC used here has been thoroughly tested in refs. [33, 34] in applications to the reaction $\gamma d \to np$ for which many experimental data exist. It provides a very satisfactory description of the data up to ~ 300 MeV.

6 Results and Discussions

Based on the described formalism, we have calculated the differential cross section (14) and the asymmetry (15) in the on-plane kinematics ($\phi_{\gamma'} = \phi_n = 0$) at a few photon energies between 100 to 400 MeV and for large angles $\theta_{\gamma'}$, which have been chosen in accordance with the kinematic region of enhanced sensitivity of γn-scattering to the difference of neutron polarizabilities $\alpha_n - \beta_n$ and sign of the π^0-decay constant, see ref. [10]. The corresponding neutron angle has been taken close to the NQFP value (12).

The relative significance of Figs. 1 a, 1 b, 2 a, and 3 a–b for the differential cross section of the reaction (1) is illustrated in Fig. 5 where the cross sections are shown corresponding to quasi-free γn scattering (QF-n, Fig. 1 a), plane-wave impulse approximation (PWIA, Figs. 1 a–b), distorted-wave impulse approximation (DWIA, Figs. 1 a, 1 b, 2 a) and total contribution (DWIA + MEC + IC, Figs. 1 a, 1 b, 2 a, 3 a, 3 b). The neutron polarizabilities are chosen to be $\alpha_n = 10$ and $\beta_n = 6$, which are close to the experimental result (5) and the dispersion predictions (3) and (6). The contribution of Fig. 1 b with photon scattering by the proton is completely negligible in the NQFP region. Nevertheless, γp scattering does essentially contribute through Fig. 2 a, which reduces the original QF-n cross section by $\simeq 27\%$ at $E_\gamma = 100$ MeV and $\theta_{\gamma'} = 135°$. The higher the energy E_γ, the smaller is the role of np rescattering, and Fig. 2 a reduces the QF-n contribution by only $\simeq 7\%$ at $E_\gamma = 400$ MeV. The correction due to MEC and IC is $\simeq -5\%$ in the kinematics shown in Fig. 5 a and it typically becomes smaller at higher energies. Beyond the NQFP region all these corrections are more important. In particular, Fig. 1 b produces the proton quasi-free peak (PQFP) at very low energies of the neutron, $E_n \lesssim 1$ MeV, which thus becomes a spectator. At small relative velocities of the np pair, which is achieved at $E_n \simeq 4$ MeV in the kinematics of Fig. 5 a, a strong peak appears due to the final-state interaction (Fig. 2 a). The differential cross section (14), being integrated over the PQFP, is almost five times greater than the corresponding integral over the NQFP, just in accordance with the ratio of γp to γn scattering cross sections at this energy. The visible smallness of the PQFP in Fig. 5 a is related with its large angular extension, $\Delta\Omega_n^{\mathrm{PQFP}} \simeq 4\pi$, whereas the angular size of the NQFP is only $\Delta\Omega_n^{\mathrm{NQFP}} \simeq 10^{-1}$.

In the case of the polarization observable, i.e. the asymmetry Σ, both corrections due to np rescattering and MEC + IC are very important in the NQFP region at the relatively low energies of $E_\gamma \simeq 100$ MeV. With increasing E_γ their significance diminishes (see Fig. 6).

Figs. 7 and 8 illustrate the sensitivity of the total results (Figs. 1 a, 1 b, 2 a, 3 a, 3 b) for the differential cross section and asymmetry with respect to the neutron electric polarizability. The predictions are given for $\alpha_n = 0$, 10, and 20 while $\alpha_n + \beta_n$ is fixed according to Eq. (6). Also, the theoretical variant with $\alpha_n = 10$ and the "wrong" sign of the π^0-decay constant, $gF \equiv g_{\pi NN} F_{\pi^0\gamma\gamma} > 0$, is shown. Evidently, the data on the differential cross section taken at various energies would enable one to determine unambiguously both the value of α_n and the sign of gF. Measurements of Σ also provide such a possibility, although the interpretation of the asymmetry in terms of the neutron polarizabilities is less reliable because of stronger dependence on rescattering and MEC + IC corrections.

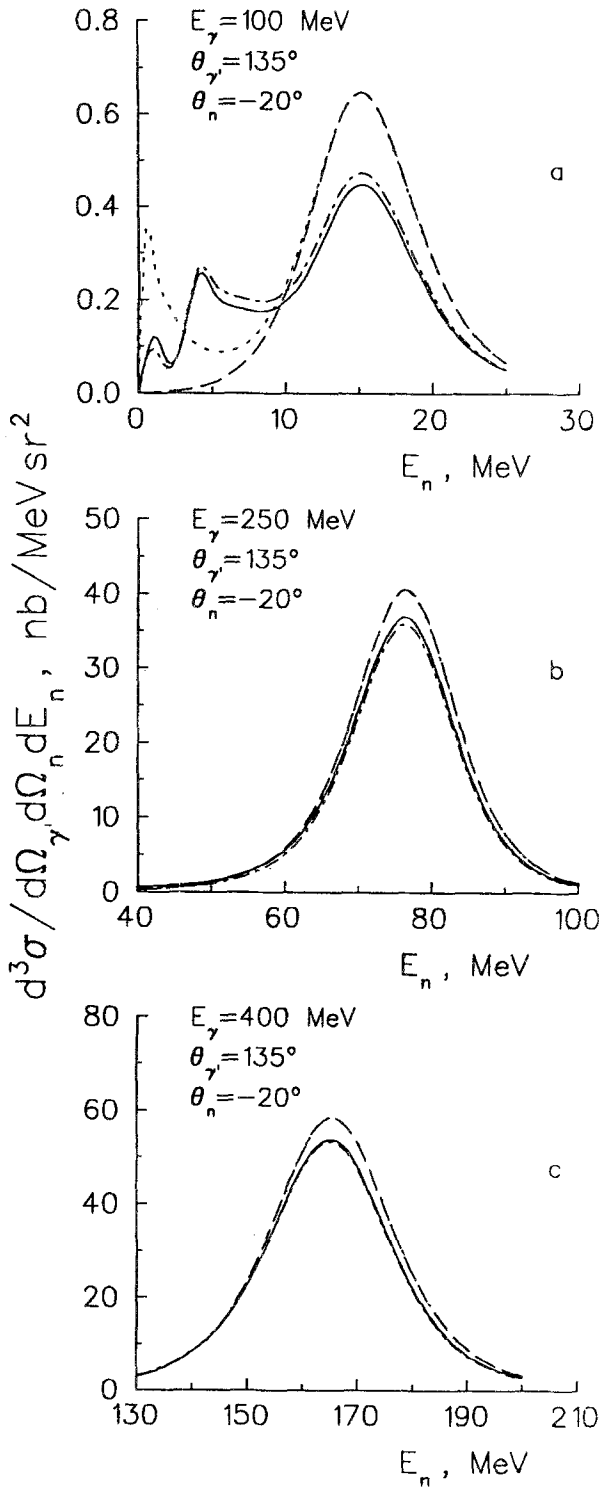

Fig. 5. The effect of different diagrams in the differential cross section. Dashed lines: the contribution of the neutron-pole diagram of Fig. 1 a. Dotted, dashed-dotted, and solid lines correspond to PWIA (Figs. 1 a, 1 b), DWIA (Figs. 1 a, 1 b, 2 a), and DWIA + MEC + IC (Figs. 1 a, 1 b, 2 a, 3 a, 3 b) contributions, respectively

If the bremsstrahlung photon beam is used for measurements and the final photon energy is not carefully measured, the visible quasi-free peak is smeared but does still survive [7]. The differential cross section with just the bremsstrahlung

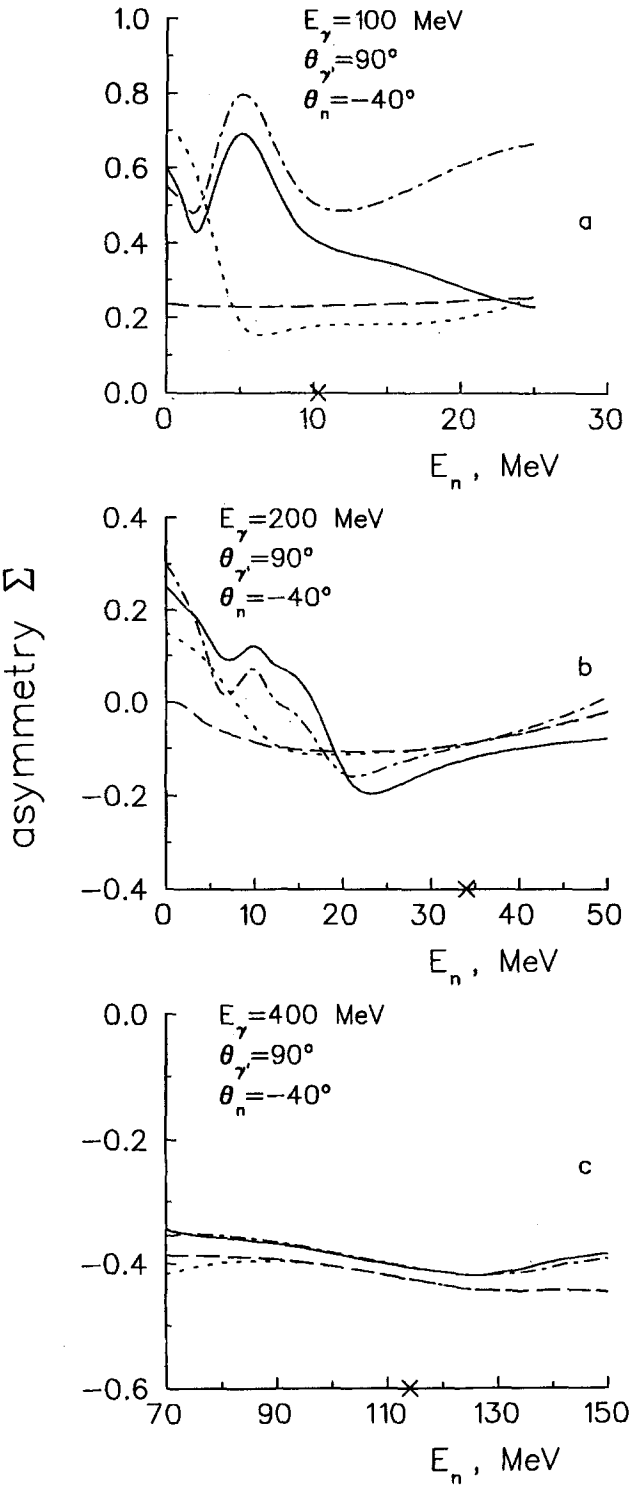

Fig. 6. The effect of different diagrams in the asymmetry Σ. Notation as in Fig. 5. The value of E_n^{peak} is shown by a cross

photons in the NQFP region has been measured in ref. [1]. The results found there agree with the present theoretical calculations and the neutron polarizabilities (3) and (5). For example, the cross section at 135° integrated over energy and angular ranges of the registered particles γ' and n is [1]

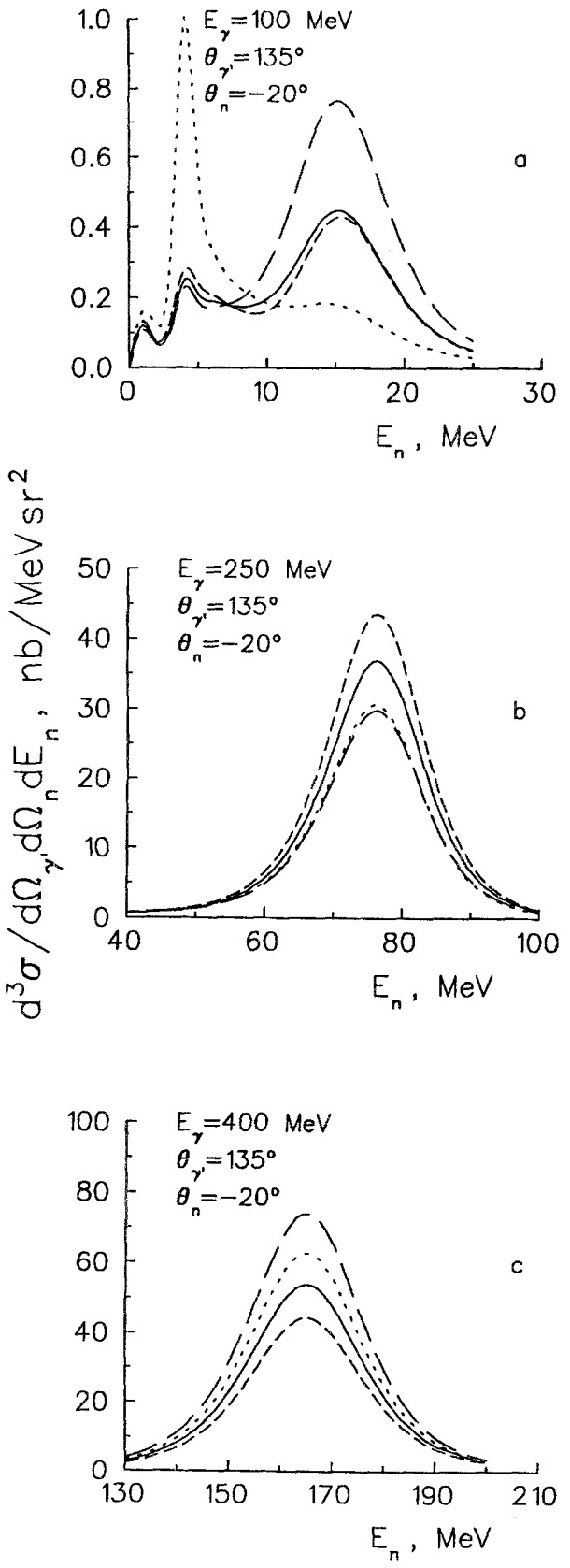

Fig. 7. Dependence of the differential cross section on the value of α_n and the sign of gF. Short-dashed, solid, and dashed lines are obtained with $gF < 0$ and $\alpha_n = 0$, 10, and 20, respectively. Dotted line: $\alpha_n = 10$ and $gF > 0$

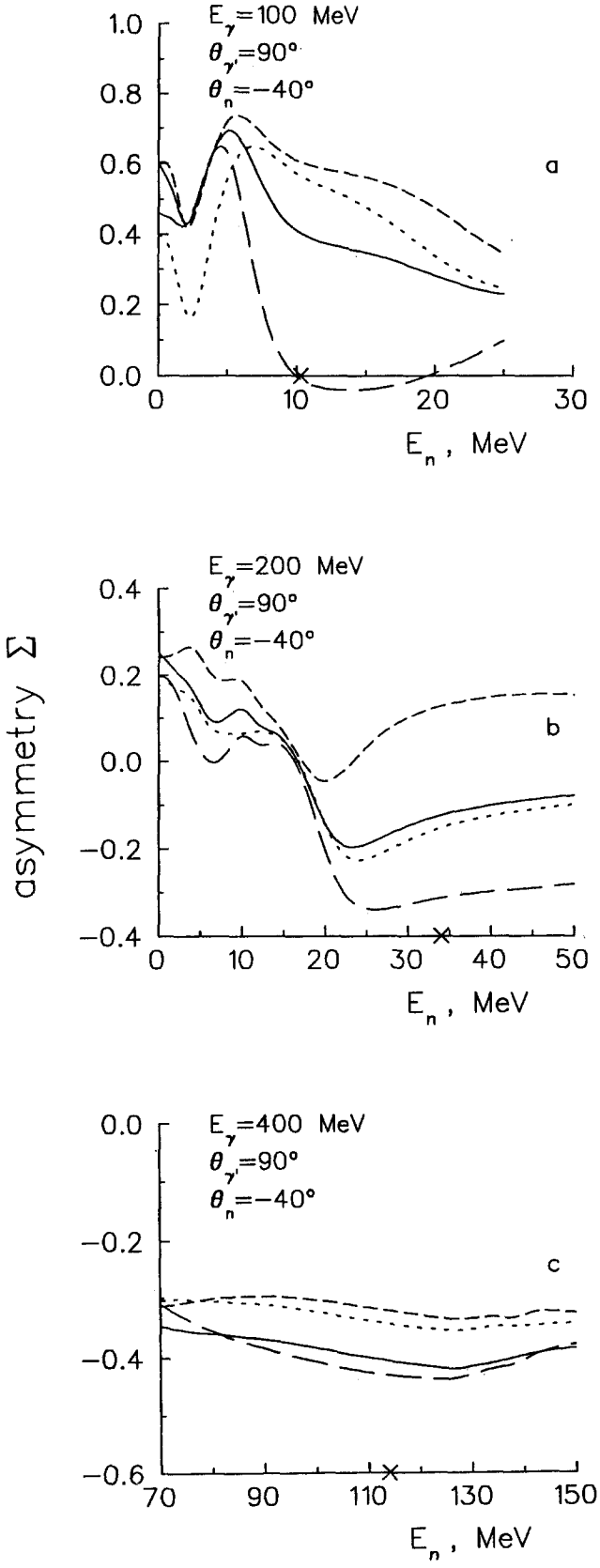

Fig. 8. Dependence of the asymmetry Σ on the value of α_n and the sign of gF. Notation as in Fig. 7. The value of E_n^{peak} is shown by a cross

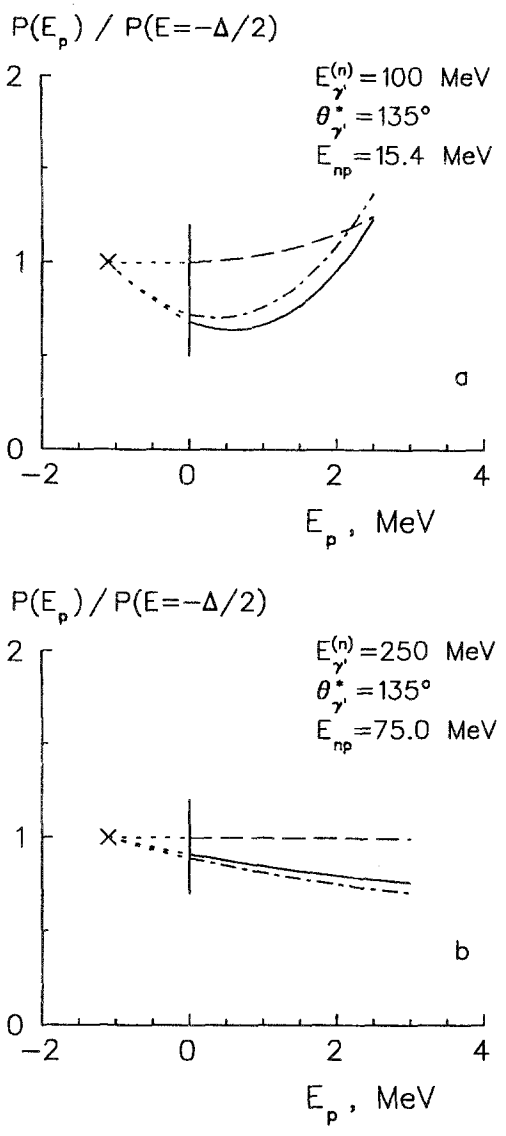

Fig. 9. The effect of different diagrams in the value of $P(E_p)$. Notation as in Fig. 5

$$\left\langle \frac{d^3\sigma}{d\Omega_{\gamma'}\, d\Omega_n\, dE_n} \right\rangle \Delta E_n = \begin{cases} 11.3 \text{ nb/sr}^2, & \text{theory with } \alpha_n = 10 \text{ and } gF < 0, \\ 12.1^{+2.9}_{-2.3} \text{ nb/sr}^2, & \text{experiment.} \end{cases} \tag{46}$$

The data obtained and compared with the theory enabled the Göttingen-Mainz group to establish the value (2) for the neutron polarizability and to support the commonly used sign of $gF < 0$.

It is interesting to discuss the possibility to determine the γn scattering cross section in a model-free way by using the standard Chew-Low extrapolation procedure. Its idea consists in the extrapolation of the measured cross section to the kinematic point $E_p = -\frac{1}{2}\Delta$, in vicinity of which the neutron pole diagram of Fig. 1 a dominates, see Eqs. (21) and (18), (19). Accordingly, we show in Fig. 9 the value

$$P(E_p) = \left[\frac{|\psi^d_{p\bar{n}}(\mathbf{p}_p)|^2}{(2\pi)^3} \frac{m E^{(n)}_{\gamma'}}{\varepsilon_p E_\gamma} \right]^{-1} \frac{d^4\sigma}{d\Omega^*_{\gamma'}\, d^3\mathbf{p}_p} \tag{47}$$

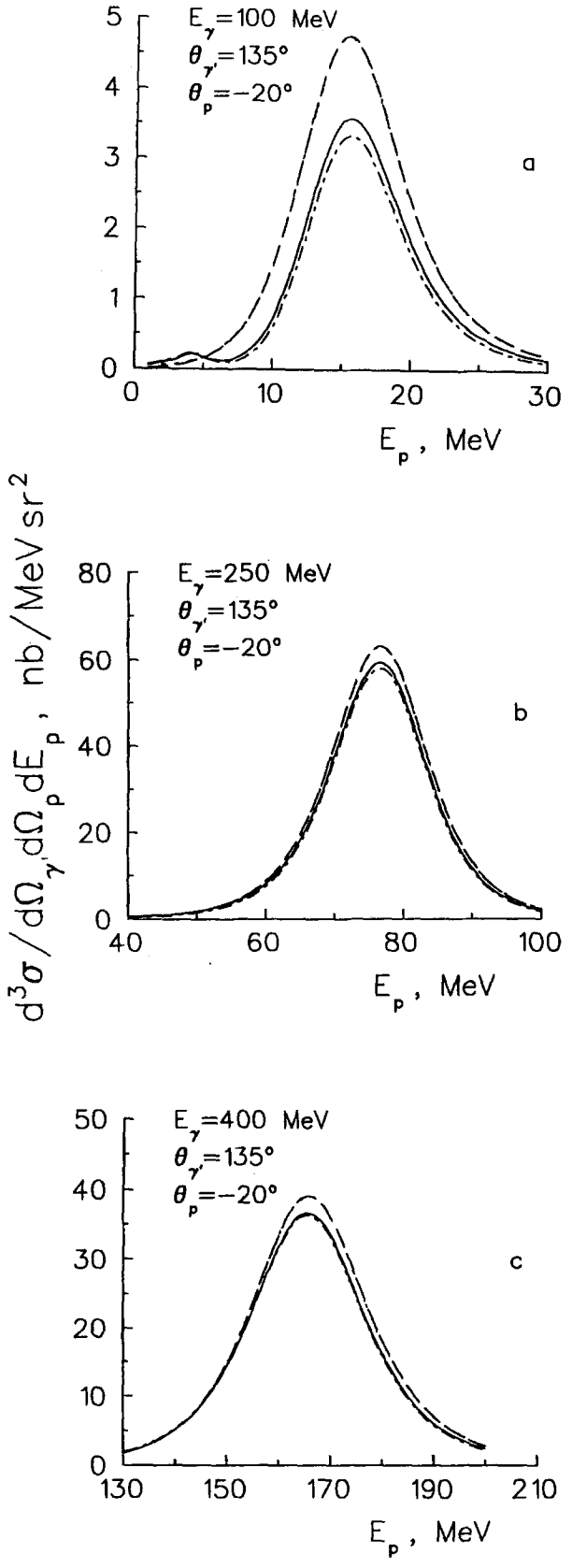

Fig. 10. The effect of different diagrams in the region of the PQFP. Dashed lines: the contribution of the proton pole, Fig. 1 b. Dashed-dotted and solid lines correspond to DWIA (Figs. 1 a, 1 b, 2 a) and DWIA + MEC + IC (Figs. 1 a, 1 b, 2 a, 3 a, 3 b) contribution, respectively. The PWIA contribution coincides with the proton-pole term within the resolution in the figure

for fixed parameters of the subprocess of γn scattering, $W^2 = m^2 + 2mE_{\gamma'}^{(n)}$ and $\theta^* = \theta_{\gamma'}^*$, and fixed relative energy $E_{np} = E_{np}^{\text{peak}} \simeq \frac{1}{2}E_n^{\text{peak}}$, which drives the rescattering magnitude. At the pole, the value of P becomes the differential c.m. cross section of γn scattering:

$$P(-\tfrac{1}{2}\Delta) = \frac{d\sigma(\gamma\tilde{n} \to \gamma' n)}{d\Omega_{\gamma'}^*}. \tag{48}$$

Since the variables W, θ^*, E_{np} and E_p do not determine unambiguously the kinematics of the reaction (1), we have the whole cone of possible directions (θ_p, ϕ_p); P is shown in Fig. 9 for one of two corresponding angles θ_p of in-plane events, the second branch having very similar features.

The theoretically expected dependence of P on E_p is non-linear, see Fig. 9, so at least an extrapolation quadratic in E_p should be used. Such an extrapolation from the region $E_p \lesssim 1$ to 2 MeV covering most of the NQFP yields rather accurate results, within $\simeq 6\%$ in the kinematics of Fig. 9 a and better than 1% in that of Fig. 9 b. Therefore, the extrapolation at fixed E_{np} indeed provides a model-independent way to find the γn scattering cross section. Note, however, that original statistical errors in the measured cross sections transform into the uncertainty in the extrapolated value of P increased by the factor of $K \approx 5$ to 10; for example, the parabola $P(E_p)$, which goes through the 3 points $P_1 = P(E_p = 0.2$ MeV), $P_2 = P(E_p = 0.8$ MeV) and $P_3 = P(E_p = 1.5$ MeV) belonging to the NQFP region, gives $P(E_p = -1.1$ MeV$) = c_1P_1 + c_2P_2 + c_3P_3$ with $c_1 \simeq 6.4$, $c_2 \simeq -8.1$ and $c_3 \simeq 2.8$, so that $K = \sqrt{c_1^2 + c_2^2 + c_3^2} \simeq 10.7$ in this case. Moreover, the extrapolation in E_p at fixed E_{np} uses only a few percent slice of all events in the NQFP region, which have almost zero projection of the proton momentum $\mathbf{p}_p$ on the direction of $\mathbf{p}_n$. All this imposes severe requirements to the precision of the measurements and hence to the total statistics. Since the integral of the cross secton (14) over the NQFP region of the neutron momentum is very small and typically ~ 1 nb/sr at $E_\gamma \sim 100$ MeV, the extrapolation method is impractical, at least at low energies, and one should explicitly consider the corrections to the neutron pole contribution as discussed in this paper.

There is an evident way to test experimentally the calculations presented for the FSI + MEC + IC effects by studying quasi-free photon scattering on protons. Since the proton polarizability and, more generally, the γp scattering amplitudes and cross sections are known better than those in the case of the neutron, the absolute predictions for the cross section $d^3\sigma/d\Omega_{\gamma'}\, d\Omega_p\, dE_p$ can be made and compared to the contribution of Compton scattering on the free proton at the same W and θ^*, see Eq. (22) and the dashed curves in Fig. 10, which are calculated with $\alpha_p = 11$; at other α_p, the dependence of the triple differential cross section on α_p essentially repeats the α_p-dependence of $d\sigma_{\gamma p}/d\Omega_{\gamma'}$ [10]. The decrease of the cross section found through the proton pole diagram by 24%, 6%, and 7% due to FSI + MEC + IC contributions is expected in the kinematics shown in Fig. 10.

7 Conclusion

The results of the presented calculations demonstrate that the differential cross section of γn scattering, the neutron polarizabilities, and the sign of gF can be

determined from the differential cross section of the reaction (1) in the NQFP region. The main correction to the dominating quasi-free neutron contribution (Fig. 1 a) is due to *np* rescattering in the final state and is calculated rather reliably, whereas more delicate corrections due to MEC and IC are small. After the pioneering measurement [1], further experiments of this type are worth being done both at low ($\sim$100 MeV) and higher ($\sim$200–250 MeV) energies to determine the neutron polarizabilities more accurately. Apparently, the accuracy of $\lesssim 5\%$ in measuring the differential cross section of the reaction (1) should be achieved to test and improve the result (5) of the measurement of α_n via nA scattering. Measurements at the photon energy $E_\gamma \sim$ 200–250 MeV are useful because the corresponding cross section is sensitive to lower values of α_n. At energies below the pion photoproduction threshold, experiments are feasible with bremsstrahlung photon beams and incomplete knowledge of the kinematics, i.e. only with the upper limitation of the final photon energy.

The asymmetry Σ is also sensitive to the values of neutron polarizabilities. Since the contributions to Σ from *np* rescattering and MEC and IC are not so small, measurements of Σ could be used as a test for theoretical treating of MEC and IC in two-current processes like the reaction (1).

Acknowledgments. Two of the authors (A. L. and V. P.) thank Profs. M. Schumacher and B. Ziegler and Drs. J. Ahrens and B. Dolbilkin for fruitful discussions and support of the method of determining the neutron polarizabilities through the process $d(\gamma, \gamma' n)p$ proposed in ref. [7] and justified in detail in this paper. The work has been supported in part by Advance Research Foundation of Belarus under contract No. F42-040, by WE-Heraeus-Stiftung, and by Deutsche Forschungsgemeinschaft.

References

1. Rose, K. W., et al.: Phys. Lett. **B234**, 460 (1990); Nucl. Phys. **A514**, 621 (1990)
2. Alexandrov, Yu. A., et al.: Pis'ma Zh. Eksp. Teor. Fiz. **4**, 196 (1966) [Sov. Phys. JETP Letters **4**, 134 (1966)]
3. Alexandrov, Yu. A., et al.: Yad. Fiz. **44**, 1384 (1986) [Sov. J. Nucl. Phys. **44**, 900 (1986)]
4. Koester, L., Waschkowski, W., Meier, J.: Z. Phys. **A329**, 229 (1988)
5. Schmiedmayer, J., Rauch, H., Riehs, P.: Phys. Rev. Lett. **61**, 1065 (1988)
6. Alexandrov, Yu. A.: Fundamental Properties of the Neutron. Oxford: Clarendon Press 1992
7. Levchuk, M. I., L'vov, A. I., Petrun'kin, V. A.: Kratk. Soobch. po Fiz. (Sov. Phys. Lebedev Inst. Reports) **2**, 3 (1985); Preprint FIAN #86. Moscow 1986
8. Shapiro, I. S.: Theory of Direct Nuclear Reactions. Moscow: Gasatomizdat 1963
9. Laget, J. M.: Phys. Rep. **69**, 1 (1981)
10. L'vov, A. I.: Yad. Fiz. **34**, 1075 (1981) [Sov. J. Nucl. Phys. **34**, 597 (1981)]; Yad. Fiz. **42**, 919 (1985) [Sov. J. Nucl. Phys. **42**, 583 (1985)]
11. Bolotov, V. N., et al.: Phys. Lett. **B243**, 308 (1990)
12. Petrun'kin, V. A.: Fiz. Elem. Chastits At. Yadra **12**, 692 (1981) [Sov. J. Part. Nucl. **12**, 278 (1981)]
13. Weiner, R., Weise, W.: Phys. Lett. **B159**, 85 (1985)
14. Schöberl, F., Leeb, H.: Phys. Lett. **B166**, 355 (1986)
15. Fiebig, H., Wilcox, W., Woloshin, R.: Nucl. Phys. **B324**, 47 (1989)
16. Bernard, V., Kaiser, N., Meissner, U.-G.: Nucl. Phys. **B373**, 346 (1992)
17. Broniowski, W., Cohen, T. D.: Phys. Rev. **D47**, 299 (1993)

18. L'vov, A. I.: Int. J. Mod. Phys. **A8**, 5267 (1993)
19. Schmiedmayer, J., Riehs, P., Harvey, J. A., Hill, N. W.: Phys. Rev. Lett. **66**, 1015 (1991)
20. Goldansky, V. I., Karpukhin, O. A., Kutsenko, A. V., Pavlovskaya, V. V.: Nucl. Phys. **18**, 473 (1960)
21. Baranov, P., et al.: Phys. Lett. **B52**, 122 (1974)
22. Federspiel, F. J., et al.: Phys. Rev. Lett. **67**, 1511 (1991)
23. Zieger, A., et al.: Phys. Lett. **B278**, 34 (1992)
24. Hallin, E. L., et al.: Phys. Rev. **C48**, 1497 (1993)
25. L'vov, A. I., Petrun'kin, V. A.: Lecture Notes in Phys. **365**, 123 (1990)
26. Nikolenko, V. G., Popov, A. B.: Z. Phys. **A341**, 365 (1992); Preprint JINR E3-92-254. Dubna 1992
27. Gal'perin, A. S., Mitsel'makher, G. V., Ol'shevskii, A. G., Pervushin, V. N.: Yad. Fiz. **32**, 1053 (1980) [Sov. J. Nucl. Phys. **32**, 545 (1980)]
28. Antipov, Yu. M., et al.: Phys. Lett. **B121**, 445 (1983); Z. Phys. **C26**, 495 (1985)
29. Starkov, N. I., Fil'kov, L. V., Tsarev, V. A.: Yad. Fiz. **36**, 1212 (1982) [Sov. J. Nucl. Phys. **36**, 707 (1982)]
30. Lacombe, M., et al.: Phys. Rev. **D12**, 1495 (1975)
31. Haidenbauer, J., Plessas, W.: Phys. Rev. **C30**, 1822 (1984); **C32**, 1424 (1985)
32. Blomqvist, I., Laget, J. M.: Nucl. Phys. **A280**, 405 (1977)
33. Laget, J. M.: Can. J. Phys. **62**, 1046 (1984)
34. Levchuk, M. I.: Preprint IP 576. Minsk 1990
35. Particle Data Group: Phys. Rev. **D45**, 11-II (1992)
36. Arndt, R. A., et al.: Phys. Rev. Lett. **65**, 157 (1990)
37. Markopoupou-Kalamara, F. G., Bugg, D. V.: Phys. Lett. **B318**, 565 (1993)
38. Pfeil, W., Schwela, D.: Nucl. Phys. **B45**, 379 (1972)
39. Moorhouse, R. G., Oberlack, H., Rosenfeld, A. H.: Phys. Rev. **D9**, 1 (1974)
40. Metkalf, W. J., Walker, R.: Nucl. Phys. **B76**, 253 (1974)
41. Arndt, R. A., et al.: Phys. Rev. **C42**, 1853 (1990); Code SAID
42. Redish, E. F., Stricker-Bauer, K.: Phys. Rev. **C36**, 513 (1987)
43. Levchuk, M. I.: (to be published)
44. Machleidt, R., et al.: Phys. Rep. **149**, 1 (1987)
45. Machleidt, R.: Adv. Nucl. Phys. **19**, 196 (1989)
46. Shirokov, Yu. M.: Zh. Eksp. Teor. Fiz. **35**, 1005 (1958) [Sov. Phys. JETP **8**, 703 (1959)]
47. Weyrauch, W.: Phys. Rev. **C41**, 880 (1990)
48. Mathiot, J.-F.: Phys. Rep. **173**, 63 (1989)

Received May 19, 1993; revised December 21, 1993; accepted for publication February 7, 1994